NASA/TM–2016-219013

A Nonlinear Modal Aeroelastic Solver for FUN3D

Benjamin D. Goldman, Robert E. Bartels, Robert T. Biedron and Robert C. Scott
Langley Research Center, Hampton, Virginia

February 2016

NASA STI Program . . . in Profile

Since its founding, NASA has been dedicated to the advancement of aeronautics and space science. The NASA scientific and technical information (STI) program plays a key part in helping NASA maintain this important role.

The NASA STI program operates under the auspices of the Agency Chief Information Officer. It collects, organizes, provides for archiving, and disseminates NASA's STI. The NASA STI program provides access to the NTRS Registered and its public interface, the NASA Technical Reports Server, thus providing one of the largest collections of aeronautical and space science STI in the world. Results are published in both non-NASA channels and by NASA in the NASA STI Report Series, which includes the following report types:

- TECHNICAL PUBLICATION. Reports of completed research or a major significant phase of research that present the results of NASA Programs and include extensive data or theoretical analysis. Includes compilations of significant scientific and technical data and information deemed to be of continuing reference value. NASA counter-part of peer-reviewed formal professional papers but has less stringent limitations on manuscript length and extent of graphic presentations.

- TECHNICAL MEMORANDUM. Scientific and technical findings that are preliminary or of specialized interest, e.g., quick release reports, working papers, and bibliographies that contain minimal annotation. Does not contain extensive analysis.

- CONTRACTOR REPORT. Scientific and technical findings by NASA-sponsored contractors and grantees.

- CONFERENCE PUBLICATION. Collected papers from scientific and technical conferences, symposia, seminars, or other meetings sponsored or co-sponsored by NASA.

- SPECIAL PUBLICATION. Scientific, technical, or historical information from NASA programs, projects, and missions, often concerned with subjects having substantial public interest.

- TECHNICAL TRANSLATION. English-language translations of foreign scientific and technical material pertinent to NASA's mission.

Specialized services also include organizing and publishing research results, distributing specialized research announcements and feeds, providing information desk and personal search support, and enabling data exchange services.

For more information about the NASA STI program, see the following:

- Access the NASA STI program home page at http://www.sti.nasa.gov

- E-mail your question to help@sti.nasa.gov

- Phone the NASA STI Information Desk at 757-864-9658

- Write to:
  NASA STI Information Desk
  Mail Stop 148
  NASA Langley Research Center
  Hampton, VA 23681-2199

NASA/TM–2016-219013

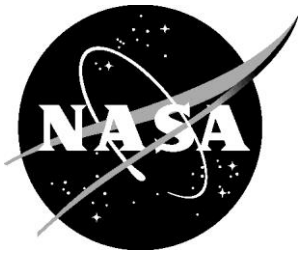

A Nonlinear Modal Aeroelastic Solver for FUN3D

Benjamin D. Goldman, Robert E. Bartels, Robert T. Biedron, and Robert C. Scott
Langley Research Center, Hampton, Virginia

National Aeronautics and
Space Administration

Langley Research Center
Hampton, Virginia 23681-2199

February 2016

Available from:

NASA STI Program / Mail Stop 148
NASA Langley Research Center
Hampton, VA 23681-2199
Fax: 757-864-6500

Abstract

A nonlinear structural solver has been implemented internally within the NASA FUN3D computational fluid dynamics code, allowing for some new aeroelastic capabilities. Using a modal representation of the structure, a set of differential or differential-algebraic equations are derived for general thin structures with geometric nonlinearities. ODEPACK and LAPACK routines are linked with FUN3D, and the nonlinear equations are solved at each CFD time step. The existing predictor-corrector method is retained, whereby the structural solution is updated after mesh deformation. The nonlinear solver is validated using a test case for a flexible aeroshell at transonic, supersonic, and hypersonic flow conditions. Agreement with linear theory is seen for the static aeroelastic solutions at relatively low dynamic pressures, but structural nonlinearities limit deformation amplitudes at high dynamic pressures. No flutter was found at any of the tested trajectory points, though LCO may be possible in the transonic regime.

Contents

1 Introduction **1**

2 Mathematical Formulation and Numerical Methods **1**
2.1 Linear Structural Dynamics 1
2.2 Nonlinear Structural Equations of Motion 3
2.2.1 Case 1: Deflection Only 3
2.2.2 Case 2: Deflection and Two In-Plane Coordinates 4
2.2.3 Case 3: Deflection and One In-Plane Coordinate 5
2.3 Nonlinear Solution Method 5

3 Determining the Nonlinear Coefficients **7**
3.1 Panels 7
3.2 Conical shells 8
3.3 Determining the Modal Basis and Nonlinear Stiffness Coefficients using Finite Element Analysis and Reduced Order Models 10

4 Input Files **10**

5 New Compiling and Linking Procedures **16**

6 Test Case: A Conical Shell Model of the NASA Hypersonic Inflatable Aerodynamic Decelerator **16**
6.1 Mathematical Formulation 17
6.2 Results 19
6.2.1 Static Aeroelastic Solutions 19
6.2.2 Dynamic Aeroelastic Solutions 23

7 Concluding Remarks **26**

References **27**

1 Introduction

Aeroelastic analysis using computational fluid dynamics (CFD) has been a subject of great interest in recent years. CFD has allowed for the most physically representative aerodynamic calculations of complex structures, making it ideal for a complete fluid-structure interaction simulation. The major challenge that remains is how to efficiently couple a complex structural system with the fluid solver, while maintaining the important physics of both the flow and structural dynamics. The NASA FUN3D code [1] is a Reynolds-Averaged Navier Stokes (RANS) CFD code in development since the 1980s. At NASA, it has been used for the design of the Mars Science Laboratory [2, 3], an aeroelastic evaluation of the Ares launch vehicle [4], and an aeroacoustic analysis of aircraft landing gear [5], among many others. Boeing, Lockheed, Cessna, and others have also used the code for new concept studies [6]. FUN3D uses unstructured grids, and solves the full viscous Navier Stokes equations to resolve the complete unsteady flowfield. Up to this point, the FUN3D aeroelastic capability allows for solutions with a modal representation of linear structural models. The internal structural dynamics equations are solved using the method of Edwards et al. [7], which is a linear state transition matrix predictor-corrector scheme for time-marching the structural modal coordinates. This approach is sufficient for calculating flutter dynamic pressures, but limit cycle amplitudes cannot be determined. Nonlinear response, including limit cycle behavior, may be of interest in cases with large deformations where linear theory no longer applies.

In this memorandum, a nonlinear modal structural solver is integrated into FUN3D. The solver is generalized to accept mode shapes and modal coefficients for a subset of structures with geometric nonlinearities. Common structures of this type are plates (panels), shells, and some wings. The nonlinear equations are solved in a predictor-corrector scheme at every time-step of the fluid integration. As a test case for the nonlinear solver, the static and dynamic aeroelastic response for a conical shell model of the NASA Hypersonic Inflatable Aerodynamic Decelerator is calculated and compared with linear theory.

2 Mathematical Formulation and Numerical Methods

In this section, a discussion of the existing linear and new nonlinear aeroelastic equations of motion and numerical solution approaches will be presented.

2.1 Linear Structural Dynamics

Before discussing the nonlinear equations of motion and new solution methods, it may be advantageous to review the existing methods for linear structural dynamics, since the nonlinear solver will make use of the general structure of this scheme. This formulation follows that of Edwards, et al. [7]. The current linear structural dynamics equations are:

$$\begin{bmatrix} 1 & 0 & 0 \\ 0 & \ddots & 0 \\ 0 & 0 & 1 \end{bmatrix} \{\ddot{q}\} + \begin{bmatrix} 2\omega_1\zeta_1 & 0 & 0 \\ 0 & \ddots & 0 \\ 0 & 0 & 2\omega_N\zeta_N \end{bmatrix} \{\dot{q}\} + \begin{bmatrix} {\omega_1}^2 & 0 & 0 \\ 0 & \ddots & 0 \\ 0 & 0 & {\omega_N}^2 \end{bmatrix} \{q\} = \begin{bmatrix} {m_1}^{-1} & 0 & 0 \\ 0 & \ddots & 0 \\ 0 & 0 & {m_N}^{-1} \end{bmatrix} \{Q\} \quad (1)$$

where q are the modal coordinates and ωn, ζn, mn are the natural frequency, damping ratio, and modal mass for the n^{th} mode, respectively. Q are the generalized aerodynamic forces defined as:

$$Q_n = q_\infty g_{refl}^2 \iint c_p \, \vec{\Psi}_n \cdot d\vec{s} - gf_0 \quad (2)$$

where q_∞ is the free-stream dynamic pressure, g_{refl} is the scale factor between CFD and structural grid units, cp is the pressure coefficient, ψn is the mode shape for the n^{th} mode, and gf_0 is a static offset for the generalized forces.

Edwards et al. [7] takes advantage of the linear structure by using a state transition matrix scheme to integrate these equations of motion. The solution, at time t, of any forced linear system is given by [8]

$$x(t) = \Phi(t)x(0) + \int_0^t \Phi\,(t\ -\ \tau)Q(\tau)d\tau \quad (3)$$

The state transition matrix Φ is:

$$\Phi = \exp(At) \quad (4)$$

where

$$A = \begin{bmatrix} 0 & I \\ M^{-1}K & 0 \end{bmatrix} \quad (5)$$

M and K are the mass and stiffness matrices, respectively. Since the equations are solved at a fixed time-step increment, the integral of the state transition matrix over interval Δt may be used:

$$\Theta_i = \int_0^{\Delta t} \exp[A(\Delta t - \tau)]\, d\tau \quad (6)$$

Solutions to Eq. 3 are computed in a predictor-corrector scheme which is consistent with the mesh-deformation procedure within FUN3D.

The predictor step is [9]:

$$\tilde{x}_{n+1} = \Phi(\Delta t)x^n + \frac{1}{2}\Theta_l(3\bar{Q}^n - \bar{Q}^{n-1}) \quad (7)$$

with

$$x = \begin{Bmatrix} q_1 \\ \dot{q}_1 \\ \vdots \\ q_N \\ \dot{q}_N \end{Bmatrix}, \bar{Q} = \begin{Bmatrix} 0 \\ Q_1 \\ \vdots \\ 0 \\ Q_N \end{Bmatrix} \tag{8}$$

A second order extrapolation has been used to determine the form of generalized forces, since $\bar{Q}^{n+1}$ is not yet known in this step.

After the predictor step, the mesh is deformed using the predicted modal solution, and the new flow field is computed and converged in several subiterations, leading to new generalized forces at step n+1.

The corrector step is:

$$x_{n+1} = \Phi(\Delta t)x^n + \frac{1}{2}\Theta_i(\bar{Q}^{n+1} + \bar{Q}^n) \tag{9}$$

Note that the both the fluid and structural solvers are second order accurate, so the aeroelastic solver is also second order accurate.

2.2 Nonlinear Structural Equations of Motion

While nonlinear structural equations can be written in many forms, here we consider only modal equations. This approach is favorable because we may take advantage of the existing modal methods for mesh deformation and aerodynamic forces currently in FUN3D. As implemented, these equations only allow for second and third order geometric nonlinearities, though source code modifications could be made rather easily to include other effects. Three different types of modal equations can be solved using this scheme, and each is described in detail in the following sections.

2.2.1 Case 1: Deflection Only

First, we consider a set of deflection equations of the form:

$$\sum_j M_{ij}\ddot{q}_j + \sum_j C_{ij}\dot{q}_j + \sum_j K_{ij}^{L,tot} q_j + K^{NL} = Q \tag{10}$$

The first three terms on the left hand side of Eq. 10 are the standard linear terms involving the mass, damping, and stiffness matrices, respectively. In this case, the form of the mass matrix and modal damping is:

$$M_{ij} = \iint m\psi_i \psi_j dA \tag{11}$$

$$C_{jj} = 2\zeta_j\omega_j \tag{12}$$

The stiffness matrix is decomposed here as:

$$K_{ij}^{L,tot} = K_{ij}^{L} + n_1 K_{ij}^{L,n_1} + n_2 K_{ij}^{L,n_1} \tag{13}$$

The constant in-plane force components n_1 and n_2 are taken out of the stiffness matrix to allow for more efficient computations at varying dynamic pressures, which may affect the membrane force distribution in some thin structures. These forces are included in the *nonlinear_structure.input* file, so the stiffness matrix does not have to be recomputed at different dynamic pressures.

The nonlinear stiffness is defined by:

$$K^{NL} = \sum_i \sum_j A_{ijk} q_i q_j + \sum_i \sum_j \sum_k B_{ijkl} q_i q_j q_k \tag{14}$$

It has been shown [10, 11, 12] that both plates and shells have geometric nonlinearities of this type when large deformations are considered.

2.2.2 Case 2: Deflection and Two In-Plane Coordinates

When formulating the large deformation structural equations for thin structures using all three displacements (deflection and two in-plane), there are two ways that the displacements maycouple. First, linear functions of in-plane displacements may appear in deflection equations and linear functions of deflection may appear in in-plane equations. Second, there is nonlinear coupling, which involves second and third order products of deflections and displacements. However, for most plate and shell structures obeying linear stress-strain laws, these coupling terms have a particularform. Nonlinear terms involving only in-plane displacements do not exist; rather, only geometric nonlinearities in deflection or products of deflection and in-plane displacements can be derived from structural theory. More specifically, equations for in-plane displacements are linear with respect to each other and nonlinear with respect to deflection. Since in-plane inertia is generally small compared to out-of-plane inertia, it may be neglected, allowing in-plane algebraic equations to be written in matrix form and solved separately from the deflection equations. We emphasize that this approximation also reduces the computational cost, since in-plane frequencies are significantly higher than out-of-plane frequencies, which would require a reduction in the time step size. With these simplifications, the nonlinear aeroelastic equations for this case are:

$$\sum_j M_{ij} \ddot{q}_j + \sum_j C_{ij}\, \dot{q}_j + \sum_j K_{ij}^{L,tot,q}\, q_j + \sum_j K_{ij}^{L,tot,a}\, a_j + \sum_j K_{ij}^{L,tot,b}\, b_j \; + \; K^{NL} = Q \tag{15}$$

$$\begin{bmatrix} LHS_{11}^{tot} & LHS_{12}^{tot} \\ LHS_{21}^{tot} & LHS_{22}^{tot} \end{bmatrix} \begin{Bmatrix} a \\ b \end{Bmatrix} = \begin{Bmatrix} RHS_a \\ RHS_b \end{Bmatrix} \tag{16}$$

$$K_{NL} = \sum_i \sum_j A_{ijk} q_i q_j + \sum_i \sum_j \sum_k B_{ijkl} q_i q_j q_k + \sum_i \sum_j D_{ijk} a_i q_j + \sum_i \sum_j E_{ijk} b_i q_j \tag{17}$$

$$RHS_a = \sum_j F_{ij}^{L,tot} q_j + \sum_i \sum_j G_{ijk} q_i q_j \tag{18}$$

$$RHS_b = \sum_j H_{ij}^{L,tot} q_j + \sum_i \sum_j L_{ijk} q_i q_j \tag{19}$$

Coefficients with "*tot*" superscripts indicate that they have the same form as Eq. 13, where constant in-plane force components are taken out of the matrix.

2.2.3 Case 3: Deflection and One In-Plane Coordinate

In cases with only one in-plane coordinate, the equations in section 2.2.2 reduce to:

$$\sum_j M_{ij} \ddot{q}_j + \sum_j C_{ij} \dot{q}_j + \sum_j K_{ij}^{L,tot,q} q_j + \sum_j K_{ij}^{L,tot,a} a_j + K^{NL} = Q \tag{20}$$

$$[LHS^{tot}] a = \sum_j F_{ij}^{L,tot} q_j + \sum_i \sum_j G_{ijk} q_i q_j \tag{21}$$

$$K_{NL} = \sum_i \sum_j A_{ijk} q_i q_j + \sum_i \sum_j \sum_k B_{ijkl} q_i q_j q_k + \sum_i \sum_j D_{ijk} a_i q_j \tag{22}$$

Equations of this form arise in symmetric analyses of shells, or in stress function formulations of thin structures [10].

2.3 Nonlinear Solution Method

To solve the nonlinear equations numerically within FUN3D, the existing predictor-corrector scheme was modified to include calls to ODEPACK [13] and LAPACK [14] routines. These FORTRAN packages were developed at national laboratories and in major university collaborations, and

have proven to be robust in their many decades of public release. ODEPACK routines, specifically DLSODE, solve first order ordinary differential equations of the form:

$$\dot{x} = f(t, x) \tag{23}$$

Equations 10, 15 and 20 may be written in a similar form, though the mass matrices are not necessarily diagonal and must be inverted. A call to the LAPACK DGESV function is used here for an LU decomposition, though a direct inverse could be computed instead. If in-plane equations arepresent, they must also be inverted at each time step using DGESV.

The state space form of the ODE in case 2 is:

$$\begin{aligned} &\frac{d}{dt}\begin{Bmatrix} q \\ M\dot{q} \end{Bmatrix} \\ &= \begin{Bmatrix} -\left(\sum_j C_{ij}\dot{q}_j + \sum_j K_{ij}^{L,tot,q}\, q_j + \sum_j K_{ij}^{L,tot,\dot{q}}\, a_j + \sum_j K_{ij}^{L,tot,b}\, b_j + K^{NL} \right) \\ + Q \end{Bmatrix} \end{aligned} \tag{24}$$

Solutions to these equations (along with Eq. 16 or Eq. 21 if in-plane displacements are considered) must be computed in a similar predictor-corrector scheme as the linear equations, in order toprovide the correct generalized coordinates for mesh deformation. The system of equations must be updated after mesh deformation with the new aerodynamic generalized forces. For convenience, calls to DLSODE were added to the existing FUN3D subroutines for the predictor and corrector steps.

Differences between the nonlinear predictor and corrector routines are as follows. In the predictor routine, the structural equations are integrated forward in one dimensional time step (*dts*) from the previous time (*t*) to the current time (*times* or *tout*). In the corrector routine, *t* = *tout*, thereby preventing the system from being integrated further in time, but allowing for the structural solution to be updated with different input parameters. In the predictor scheme, the generalized aerodynamic forces are those at the previous time step. In the corrector, the post-mesh deformation forces are used, requiring the structural solution to be updated. In both schemes, DLSODE calls the subroutine *eqsys*, which contains the nonlinear equations of motion. It is rather lengthy and not provided here, but it can be found in the FUN3D source distribution (within source file *subode*.*F*90).

3 Determining the Nonlinear Coefficients

The nonlinear coefficient matrices and tensors for Eqs. 10 - 22 may be determined using a variety of methods. First, we consider quasi-analytical approaches for a subset of structures that may be of interest for aerospace applications.

3.1 Panels

The large deformations of a plate (panel) are governed by Von Karman's equations [10]:

$$D\nabla^4 w = \frac{\partial^2 F}{\partial y^2}\frac{\partial^2 w}{\partial x^2} + \frac{\partial^2 F}{\partial x^2}\frac{\partial^2 w}{\partial y^2} - 2\frac{\partial^2 F}{\partial x \partial y}\frac{\partial^2 w}{\partial x \partial y} - m\frac{\partial^2 w}{\partial t^2} - \Delta p \tag{25}$$

$$\frac{\nabla^4 F}{Eh} = \left(\frac{\partial^2 w}{\partial x \partial y}\right)^2 - \left(\frac{\partial^2 w}{\partial x^2}\right)\left(\frac{\partial^2 w}{\partial y^2}\right) \tag{26}$$

where w is the deflection and F is the airy stress function, which defines the in-plane stresses.

Assuming modal series of the form:

$$\begin{aligned} w &= \sum_m q_m \psi_m(x,y) \\ F &= \sum_r a_r \varphi_r(x,y) \end{aligned} \tag{27}$$

and applying the Galerkin averaging procedure, a set of nonlinear aeroelastic modal equations can be derived which have the form of Eqs. 20-22. The mode shapes ψ_m and ϕ_r are usually assumed functions that satisfy the boundary conditions. A detailed derivation of these equations can be found in Ref. [10].

3.2 Conical shells

Another structure of interest for aerospace applications is the conical shell. Nonlinear behavior of shells may include circumferential buckling at pressures above the linear buckling pressure, coupling between multiple circumferential modes during flutter, as well as limit cycle oscillations. There are many ways to formulate the shell equations using quasi-analytical methods. Here, we consider the Rayleigh-Ritz approach. A detailed derivation is provided in Ref. [12], but a brief summary of the mathematical formulation is given below.

The nonlinear Donnell strain-displacement relations are given by:

$$\begin{aligned}\varepsilon_y &= \frac{\partial u}{\partial y} + \frac{1}{2}\left(\frac{\partial w}{\partial y}\right)^2 \\ \varepsilon_\theta &= \frac{u - w\cot\beta}{y} + \frac{1}{y}\frac{\partial v}{\partial \phi} + \frac{1}{2y^2}\left(\frac{\partial w}{\partial \phi}\right)^2 \\ \varepsilon_{y\theta} &= \frac{\partial v}{\partial y} - \frac{v}{y} + \frac{1}{y}\frac{\partial u}{\partial \phi} + \frac{1}{y}\frac{\partial w}{\partial y}\frac{\partial w}{\partial \phi}\end{aligned} \tag{28}$$

The curvatures are linear functions of deflection (and its derivatives):

$$\begin{aligned}\chi_y &= \frac{\partial^2 w}{\partial y^2} \\ \chi_\theta &= \frac{1}{y}\frac{\partial w}{\partial y} + \frac{1}{y^2}\frac{\partial^2 w}{\partial \phi^2} \\ \chi_{y\theta} &= \frac{1}{y}\frac{\partial^2 w}{\partial y \partial \phi} - \frac{1}{y^2}\frac{\partial w}{\partial \phi}\end{aligned} \tag{29}$$

The force and moment relations are:

$$\begin{aligned}N_y &= \frac{E_y h}{1 - v_y v_\theta}\left(\varepsilon_y + v_\theta \varepsilon_\theta\right) \\ N_\theta &= \frac{E_\theta h}{1 - v_\theta v_y}\left(\varepsilon_\theta + v_y \varepsilon_y\right) \\ N_{y\theta} &= G_{y\theta} h \varepsilon_{y\theta}\end{aligned} \tag{30}$$

$$\begin{aligned}M_y &= -D_y\left(\chi_y + v_\theta \chi_\theta\right) \\ M_\theta &= -D_\theta\left(\chi_\theta + v_y \chi_y\right) \\ M_{y\theta} &= -D_{y\theta}\chi_{y\theta}\end{aligned} \tag{31}$$

The displacements *u*, *v*, and *w* are in the in-plane axial, in-plane circumferential, and out-of- plane directions, respectively. The angle $\varphi = \theta \sin\beta$, where θ is the circumferential angle and β is the shell half-cone angle.

The strain energy is constructed by integrating over the entire shell surface the forces times strains and moments times curvatures:

$$U_S = \frac{1}{2}\int_{y1}^{y2}\int_0^{2\pi}\left(N_y\varepsilon_y + N_\theta\varepsilon_\theta + N_{y\theta}\varepsilon_{y\theta} - M_y\chi_y - M_\theta\chi_\theta - 2M_{y\theta}\chi_{y\theta}\right)yd\phi dy \tag{32}$$

The membrane energy associated with static axial or pressure loading is given by McNeal [15]:

$$U_{IS} = \frac{1}{2}\int_{y1}^{y2}\int_0^{2\pi}\left(N^a_{y,tot}\Theta_\theta^2 + N^a_{\theta,tot}\Theta_y^2 + \left\{N^a_{y,tot} + N^a_{\theta,tot}\right\}\Theta_n^2\right)yd\phi dy\ . \tag{33}$$

Here the strain rotation vectors are:

$$\begin{aligned}\Theta_\theta &= -\frac{\partial w}{\partial y}\\ \Theta_y &= \frac{v}{y\tan\beta} - \frac{1}{y}\frac{\partial w}{\partial \phi}\\ \Theta_n &= \frac{v}{2y} + \frac{1}{y}\frac{\partial v}{\partial y} - \frac{1}{2y}\frac{\partial u}{\partial \phi}\end{aligned} \tag{34}$$

The applied in-plane forces are related to the static pressure and tension by the relation

$$\begin{aligned}N^a_{y,tot} &= -\frac{y\tan\beta p_s}{2} - N^a_y\\ N^a_{\theta,tot} &= -y\tan\beta p_s\end{aligned} \tag{35}$$

The total kinetic energy, neglecting rotatory inertia, is:

$$T = \frac{m}{2}\int_{y1}^{y2}\int_0^{2\pi}\left[\left(\frac{\partial u}{\partial t}\right)^2 + \left(\frac{\partial v}{\partial t}\right)^2 + \left(\frac{\partial w}{\partial t}\right)^2\right]yd\phi dy \tag{36}$$

The three shell displacements are expanded using modal series with summations over both the axial and circumferential modes. A double summation is necessary since the structural nonlinearities introduce coupling among the circumferential modes (usually sinusoidal functions that satisfy the periodicity conditions around the circumference). The axial modes may be any functions that satisfy the geometric boundary conditions. Sine functions can be used for simply-supported boundaries, where all three displacements vanish at the shell edges. The modal expansions are:

$$\begin{aligned}u(y,\theta,t) &= \sum_m\sum_n a_{mn}(t)\cos n\phi\ \psi_m(y)\\ v(y,\theta,t) &= \sum_m\sum_n b_{mn}(t)\sin n\phi\ \psi_m(y)\\ w(y,\theta,t) &= \sum_m\sum_n c_{mn}(t)\cos n\phi\ \psi_m(y)\end{aligned} \tag{37}$$

After substituting Eq. 37 into Eqs. 32 - 36, constructing the Lagrangian, and applying the Lagrange equation for each modal coordinate, a system of differential-algebraic equations in the form of Eqs. 15-19 is obtained.

3.3 Determining the Modal Basis and Nonlinear Stiffness Coefficients using Finite Element Analysis and Reduced Order Models

While semi-analytical methods like Galerkin and Rayleigh-Ritz are relatively easy to use, they can only be applied to certain structures with relatively simple geometry and boundary conditions. For more complex structures, it may be necessary to use some form of finite element analysis to extract the modal basis and nonlinear stiffness coefficients. In this section, a brief summary of previous investigations on this topic will be presented.

Rizzi and Przekop [16] developed a reduced order method using system identification to calculate the nonlinear modal basis for arbitrary structures. By using proper orthogonal decomposition (POD) to capture the nonlinear dynamic response, and then matching the proper orthogonal modes to the natural (normal modes), a sufficient basis can be determined.

Muravyov and Rizzi [17,18] evaluated the second and third order nonlinear stiffness coefficients in MSC NASTRAN. This was accomplished by prescribing a set of particular displacement fields, resulting in a set of inverse linear and nonlinear static problems. The nonlinear forces and unknown nonlinear coefficients can then be determined. For a set of test cases, it was found that static deformations using this method were in agreement with the NASTRAN direct nonlinear static solution 106.

Radu et al. [19] used similar methods to determine the nonlinear modes and stiffnesses for a plate subject to thermo-acoustic loading. While a quasi-analytical method could be used in this case, they validated their reduced order model with a direct solution in NASTRAN. Philpot et al. [20] considered a joined-wing configuration, and also found good agreement with the direct NASTRAN result.

4 Input Files

The nonlinear aeroelastic solver requires two input files: *moving_body.input* and *nonlinear_structure.input*. The *moving_body.input* file is the same namelist input file used for linear aeroelasticity, though some modifications are required for the nonlinear solver. The following changes have been implemented in the &*aeroelastic_modal_data* namelist section (only):

1. *structure_type* = 0

This new variable defaults to 0 for the linear solver, and must be set to 1 to use the nonlinear solver. In the latter case, the *nonlinear_structure.input* file must be provided in the run directory.

2. *freq*(:, 1) = 0

While the modal frequencies in this case are not used to construct the stiffness matrix, they are required if modal damping is to be applied. Since frequencies are not normally known in nonlinear analyses, they can be set to any arbitrary value here. The damping ratio will then scale the total modal damping (see Eq. 12).

3. *gmass*(:, 1) = 0

The generalized mass is not used in the nonlinear solver.

4. *damp*(:, 1) = 0
The damping ratio is used to construct the modal damping matrix (see Eq. 12).

5. *gvel*0(:, 1) = 0, *gdisp*0(:, 1) = 0
The initial velocities and displacements are used to specify the initial conditions in the non- linear solver. The initial conditions must be commensurate with the DLSODE tolerance parameters set in the nonlinear_structure.input file.

The *nonlinear_structure.input* file is a standard space delimited text file that contains parameters for the nonlinear solver as well as the matrix and tensor coefficients. It must be formatted exactly as indicated below, in the exact same order, or else an error will be returned. Listing array values requires that each value be entered on a separate line along with the corresponding indices. If a coefficient matrix is not required for a particular analysis, it should still be entered in the input file with zero values. The format of the input files are different for each of the equation types, and are given below. Parameter and variable definitions are provided in Table 1.

For the deflection equation only (case 1):

```
%nonlinear equation type (1, 2, or 3)
1
%In-plane forces n1, n2
n1 n2
% ODE parameters itol rtol atoll itask istate iopt lrw liw mf
itol rtol atoll itask istate iopt lrw liw mf
!matrix coefficients: indx1 indx2…indxN value
i     j            mass (i, j)      %i = 1:nmodes, j = 1:nmodes
i     j            Kl (i, j)        %i = 1:nmodes, j = 1:nmodes
i     j    k       Anl (i, j, k)    %i = 1:nmodes, j=1:nmodes    k = 1:nmodes
i     j    k    l  Bnl (i, j, k, l) %i = 1:nmodes, j=1:nmodes    k = 1:nmodes, l =1:nmodes
i     j            Kln1 (i, j)      %i = 1:nmodes, j = 1:nmodes
i     j            Kln2 (i, j)      %i = 1:nmodes, j = 1:nmodes
```

For deflection and two in-plane coordinates (case 2):

```
% nonlinear equation type (1, 2, 3)
2
% number of modes for in–plane coords. a & b, in–plane forcesn1, n2
nmodes_a nmodes_b n1 n2
% initial conditions in the in–plane coordinates a and b
i a(i)      %i=1:nmodes _a
i b(i)      %i=1:nmodes _b
% itol rtol atoll itask istate iopt lrw liw mf
itol rtol atoll itask istate iopt lrw liw mf
!matrix coefficients: indx1 indx2…indxN value
i       j         mass (i,j)            %i = 1:nmodes, j = 1:nmodes
i       j         Kl (i,j)              %i = 1:nmodes, j = 1:nmodes
i   j   k         Anl (i,j,z)     %i = 1:nmodes,    j = 1:nmodes,   k = 1:nmodes
```

```
14  i  j  k  l  Bnl (i,j,k,l)  %i = 1:nmodes,   j = 1:nmodes,   k = 1:nmodes,  l = 1:nmodes
15  i  j        Kln1 (i,j)     %i = 1:nmodes,   j = 1:nmodes
16  i  j        Kln2 (i,j)     %i = 1:nmodes,   j = 1:nmodes
17  i  j        Kla (i,j)      %i = 1:nmodes,   j = 1:nmodes   nmodes_a
18  i  j        Klb (i,j)      %i = 1:nmodes,   j = 1:nmodes   nmodes_b
19  i  j        Fl (i,j)       %i = 1:nmodes_a, j = 1:nmodes
20  i  j        Hl (i,j)       %i = 1:nmodes_b, j = 1:nmodes
21  i  j        lhsab (i,j)    %i = 1:nmodes_a + nmodes_b,   j = 1:nmodes_a + nmodes_b
22  i  j  k     Dnl (i,j,k)    %i = 1:nmodes,   j = 1:nmodes,   k = 1:nmodes_a
23  i  j  k     Enl (i,j,k)    %i = 1:nmodes,   j = 1:nmodes,   k = 1:nmodes_b
24  i  j  k     Gnl (i,j,k)    %i = 1:nmodes_a, j = 1:nmodes,   k = 1:nmodes
25  i  j  k     Lnl (i,j,k)    %i = 1:nmodes_b, j = 1:nmodes,   k = 1:nmodes
26  i  j        Klan1 (i,j)    %i = 1:nmodes,   j = 1:nmodes   nmodes_a
27  i  j        Klan2 (i,j)    %i = 1:nmodes,   j = 1:nmodes   nmodes_a
28  i  j        Klbn1 (i,j)    %i = 1:nmodes,   j = 1:nmodes   nmodes_b
29  i  j        Klbn2 (i,j)    %i = 1:nmodes,   j = 1:nmodes   nmodes_b
30  i  j        Fln1 (i,j)     %i = 1:nmodes_a, j = 1:nmodes
31  i  j        Fln2 (i,j)     %i = 1:nmodes_a, j = 1:nmodes
32  i  j        Hln1 (i,j)     %i = 1:nmodes_b, j = 1:nmodes
33  i  j        Hln1 (i,j)     %i = 1:nmodes_b, j = 1:nmodes
34  i  j        lhsabn1 (i,j)  %i = 1:nmodes_a + nmodes_b,   j = 1:nmodes_a + nmodes_b
35  i  j        lhsabn2 (i,j)  %i = 1:nmodes_a + nmodes_b,   j = 1:nmodes_a + nmodes_b
```

For deflection and one in-plane coordinate (case 3):

```
1   Nonlinear equation type (1, 2 or 3)
2   3
3   % number of modes for in–plane coords a, in–plane forcesn1, n2
4   nmodes_a n1 n2
5   % initial conditions in the in–plane coordinate a
6   i a(i)     %i=1:nmodes_a
7   % itol rtol atoll itask istate iopt lrw liw mf
8   itol rtol atoll itask istate iopt lrw liw mf
9   ! matrix coefficients: indx1 indx2…indxN value
10  i  j        mass (i,j)     %i = 1:nmodes,   j = 1:nmodes
11  i  j        Kl (i,j)       %i = 1:nmodes,   j = 1:nmodes
12  i  j  k     Anl (i,j,z)    %i = 1:nmodes,   j = 1:nmodes,   k = 1:nmodes
13  i  j  k  l  Bnl (i,j,k,l)  %i = 1:nmodes,   j = 1:nmodes,   k = 1:nmodes,  k = 1:nmodes
14  i  j        Kln1 (i,j)     %i = 1:nmodes,   j = 1:nmodes
15  i  j        Kln2 (i,j)     %i = 1:nmodes,   j = 1:nmodes
16  i  j        Kla (i,j)      %i = 1:nmodes,   j = 1:nmodes   nmodes_a
17  i  j        Fl (i,j)       %i = 1:nmodes_a, j = 1:nmodes
18  i  j        lhsab (i,j)    %i = 1:nmodes_a, j = 1:nmodes_a
19  i  j  k     Dnl (i,j,k)    %i = 1:nmodes,   j = 1:nmodes,   k = 1:nmodes_a
20  i  j  k     Gnl (i,j,k)    %i = 1:nmodes_a, j = 1:nmodes,   k = 1:nmodes
21  i  j        Klan1 (i,j)    %i = 1:nmodes,   j = 1:nmodes   nmodes a_
22  i  j        Klan2 (i,j)    %i = 1:nmodes,   j = 1:nmodes   nmodes a_
23  i  j        Fln1 (i,j)     %i = 1:nmodes_a, j = 1:nmodes
24  i  j        Fln2 (i,j)     %i = 1:nmodes_a, j = 1:nmodes
25  i  j        lhsabn1 (i,j)  %i = 1:nmodes_a, j = 1:nmodes_a
26  i  j        lhsabn2 (i,j)  %i = 1:nmodes_a, j = 1:nmodes_a
```

Table 1: Parameter definitions for the *nonlinear_structure.input* file.

Variable	Description
nonlin_eq_type	Nonlinear equation type, = 1, 2, or 3 (refers to cases in sc. 2.2)
nmodes	Total number of deflection modes (provided in *moving_body.input*)
nmodes_a	Total number of in-plane modes for coordinate a
nmodes_b	Total number of in-plane modes for coordinate b
n1	In-pane force coefficient 1
n2	In-pane force coefficient 2
itol	See appendix or ODEPACK documentation
rtol	See appendix or ODEPACK documentation
atol	See appendix or ODEPACK documentation
itask	See appendix or ODEPACK documentation
istate	See appendix or ODEPACK documentation
iopt	See appendix or ODEPACK documentation
lrw	See appendix or ODEPACK documentation
mf	See appendix or ODEPACK documentation
mass	Mass matrix (not generalized mass)
Kl	Linear stiffness matrix (third term in Eqs. 10 and 15)
Anl	Nonlinear stiffness tensor (first term in Eqs. 14 and 17)
Bnl	Nonlinear stiffness tensor (first term in Eqs. 14 and 17)
Kln1	Stiffness matrix multiplied by n1 (Eq. 13)
Kln2	Stiffness matrix multiplied by n2 (Eq. 13)
Kla	Linear stiffness matrix for the in-plane coord. a (fourth term in Eq. 17)
Klb	Linear stiffness matrix for the in-plane coord. b (fourth term in Eq. 17)
Fl	Linear stiffness matrix in the RHS of the in-plane system (first term in Eq. 18)
Hl	Linear stiffness matrix in the RHS of the in-plane system (first term in Eq. 19)
lhsab	Left hand side of the in-pane system (Eq. 16)
Dnl	Nonlinear coupling stiffness tensor (Third term in Eq. 17)
Enl	Nonlinear coupling stiffness tensor (Fourth term in Eq. 17)
Gnl	Nonlinear stiffness tensor (Second term in Eq. 18)
Lnl	Nonlinear stiffness tensor (Second term in Eq. 19)
Klan1	Stiffness matrix multiplied by n1 ($Kla^{tot} = Kla + n1 * Klan1 + n2 * Klan2$)
Klan2	Stiffness matrix multiplied by n2 ($Kla^{tot} = Kla + n1 * Klan1 + n2 * Klan2$)
Klbn1	Stiffness matrix multiplied by n1 ($Klb^{tot} = Klb + n1 * Klbn1 + n2 * Klbn2$)
Klbn2	Stiffness matrix multiplied by n2 ($Klb^{tot} = Klb + n1 * Klbn1 + n2 * Klbn2$)
Fln1	Stiffness matrix multiplied by n1 ($F^{tot} = F + n1 * Fn1 + n2 * Fn2$)
Fln2	Stiffness matrix multiplied by n2 ($F^{tot} = F + n1 * Fn1 + n2 * Fn2$)
Hln1	Stiffness matrix multiplied by n1 ($H^{tot} = H + n1 * Hn1 + n2 * Hn2$)
Hln2	Stiffness matrix multiplied by n2 ($H^{tot} = H + n1 * Hn1 + n2 * Hn2$)
lhsabn1	LHS multiplied by n1 ($lhsab^{tot} = lhsab + n1 * lhsabn1 + n2 * lhsabn2$)
lhsabn2	LHS multiplied by n2 ($lhsab^{tot} = lhsab + n1 * lhsabn1 + n2 * lhsabn2$)

To demonstrate more clearly the construction of a *nonlinear_structure.input* file, consider the following unrealistic 2-mode example for Case 1. The coefficients have no physical significance, rather, they are composed of unique digits that will assist in identifying the correct entries in the input file. The coefficients are:

$M_{11} = 1$ $M_{12} = 2$ $M_{21} = 3$ $M_{22} = 4$

$K_{11}^{L} = 5$ $K_{12}^{L} = 6$ $K_{21}^{L} = 7$ $K_{22}^{L} = 8$

$A_{111} = 9$ $A_{212} = 10$ $A_{121} = 11$ $A_{122} = 12$

$A_{211} = 13$ $A_{212} = 14$ $A_{221} = 15$ $A_{222} = 16$

$n1 = 100$

$n2 = 200$

$K_{11}^{L,n1} = 33$ $K_{12}^{L,n1} = 34$ $K_{21}^{L,n1} = 35$ $K_{22}^{L,n1} = 36$

$K_{11}^{L,n2} = 37$ $K_{12}^{L,n2} = 38$ $K_{21}^{L,n2} = 39$ $K_{22}^{L,n2} = 40$

$B_{1111} = 17$ $B_{1112} = 18$ $B_{1121} = 19$ $B_{1122} = 20$

$B_{1211} = 21$ $B_{1212} = 22$ $B_{1221} = 23$ $B_{1122} = 24$

$B_{2111} = 25$ $B_{2112} = 26$ $B_{2121} = 27$ $B_{2122} = 28$

$B_{2211} = 29$ $B_{2212} = 30$ $B_{2221} = 31$ $B_{2222} = 32$

The corresponding nonlinear_structure.input file is shown:

```
%nonlinear equation type (1, 2 or 3)
1
%In-plane forces n1 n2
100 200
% ODE parameters: itol rtol atoll itask istate iopt lrw liw mf
1 1E-6 1E-6 1 1 0 52 20 10
! matrix coefficients:  indx1  indx2 ... indxN                    value
1       1                   1   %M
1       2                   2
2       1                   3
2       2                   4
1       1                   5   %Kl
1       2                   6
2       1                   7
2       2                   8
1       1       1             9 %Anl
1       1       2            10
1       2       1            11
1       2       2            12
2       1       1            13
2       1       2            14
2       2       1            15
2       2       2            16
1       1       1       1    17          %Bnl
1       1       1       2    18
1       1       2       1    19
1       1       2       2    20
1       2       1       1    21
1       2       1       2    22
1       2       2       1    23
1       2       2       2    24
2       1       1       1    25
2       1       1       2    26
2       1       2       1    27
2       1       2       2    28
2       2       1       1    29
2       2       1       2    30
2       2       2       1    31
2       2       2       2    32
1       1                    33          %Kln1
1       2                    34
2       1                    35
2       2                    36
1       1                    37          %Kln2
1       2                    38
2       1                    39
2       2                    40
```

5 New Compiling and Linking Procedures

To compile FUN3D with the nonlinear solver routines, it is necessary to include the ODEPACK and LAPACK libraries. Several modifications to the configuration scripts are also required. The detailed procedure to build the libraries can be obtained on request.

6 Test Case: A Conical Shell Model of the NASA Hypersonic Inflatable Aerodynamic Decelerator

In this section, an elastically-supported conical shell structural model of the flexible thermal protection system (TPS) on the NASA Hypersonic Inflatable Aerodynamic Decelerator (HIAD) is considered in FUN3D. The HIAD structure is given in Fig. 1, showing the inflated toroid substructure and outer TPS shell. Aeroelastic solutions of the TPS are computed using both the linear and nonlinear solvers, and results are compared.

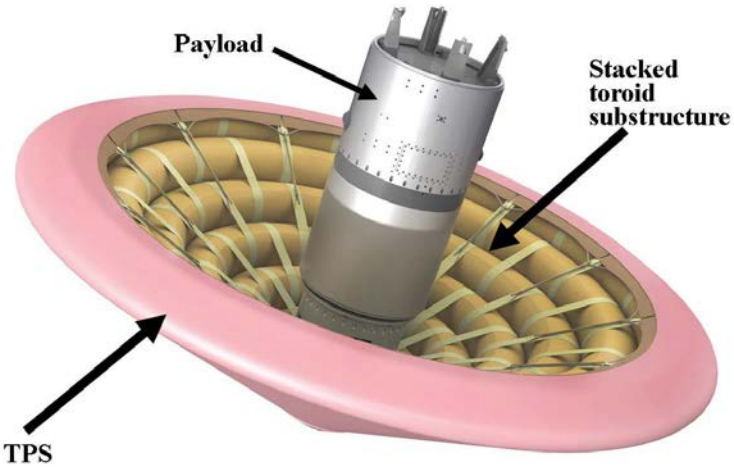

Figure 1: HIAD vehicle used in the Inflatable Re-Entry Vehicle Experiment [23].

The CFD volume mesh for this configuration is shown in Fig 2. This mesh contains the complete geometry for the 6-meter 60 degree vehicle with centerbody. The boundary condition on the HIAD surface is the typical no-slip condition, while the edges of the computational domain have inflow/outflow Riemann Invariant boundary conditions. The surface mesh of the HIAD is composed of several patches, but only a small subset of these patches is of interest for the present aeroelastic analysis. The HIAD nose cap, underside surface, and centerbody are assumed to be rigid, while the aeroshell surface is allowed to deform. The shape of this surface is a perfect conical shell, therefore, its structural dynamics can be modeled using conical shell theory. The surface mesh for this region of interest is given in Fig. 3, and the corresponding elastically-supported conical shell structural model is given in Fig. 4. The elastic supports approximate the toroids in a linear sense, and the model does not account for the static deformation of the substructure.

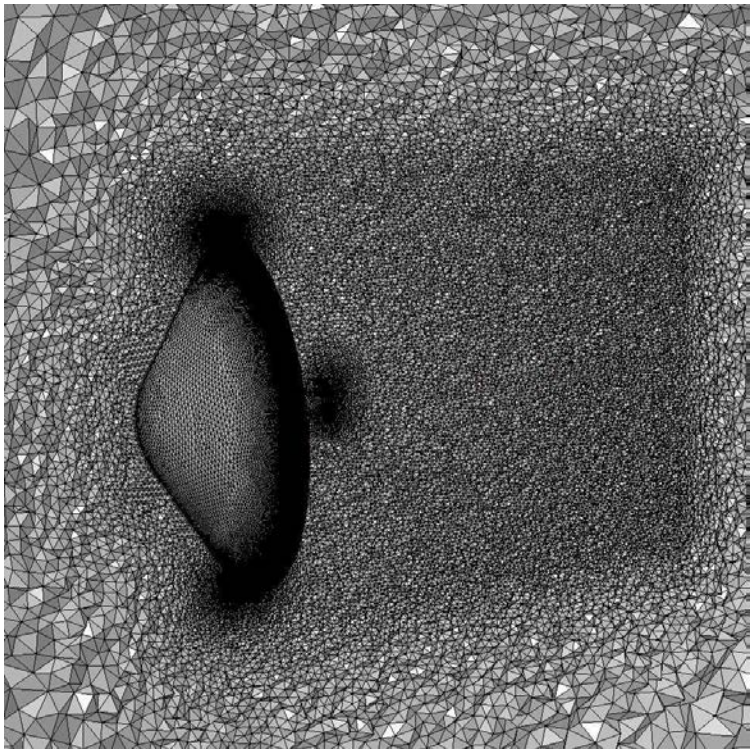

Figure 2: HIAD volume mesh (cross section at domain center).

6.1 Mathematical Formulation

This configuration may be analyzed using either linear or nonlinear structural dynamics. Results from both analyses will be discussed and compared. In the linear case, Donnell shell theory and the Rayleigh-Ritz method are used to derive a system of linear equations for the structural dynamics, which have been solved previously. The natural modes and natural frequencies of the shell were calculated and provided to FUN3D for aeroelastic analysis using the state transition matrix scheme. In this case, the shell is not pre-stressed, so membrane effects due to mean flow static pressure are neglected in the natural mode calculation. In the nonlinear case, the Rayleigh- Ritz method was used along with (geometrically nonlinear) Donnell shell theory to derive a nonlinear differential-algebraic system in the form of Eqs. 15 and 16. Sinusoidal axial modes have been used, satisfying the simply-supported boundary conditions. A plot of the first sinusoidal mode is shown in Fig. 5.

The first 30 symmetric natural modes were included for the linear analysis, and 40 assumed sinusoidal modes, (20 axial and 2 circumferential) were used for the nonlinear analysis. Both the symmetric modes and the asymmetric buckling modes have been included. It is necessary to include the buckling mode because a previous investigation [12] with piston theory indicated that the buckling mode couples with the flutter mode after the onset of nonlinear flutter at large deformations. For the 6-meter, 60 degree elastically-supported shell used in this analysis, *kbuckling* = 47.

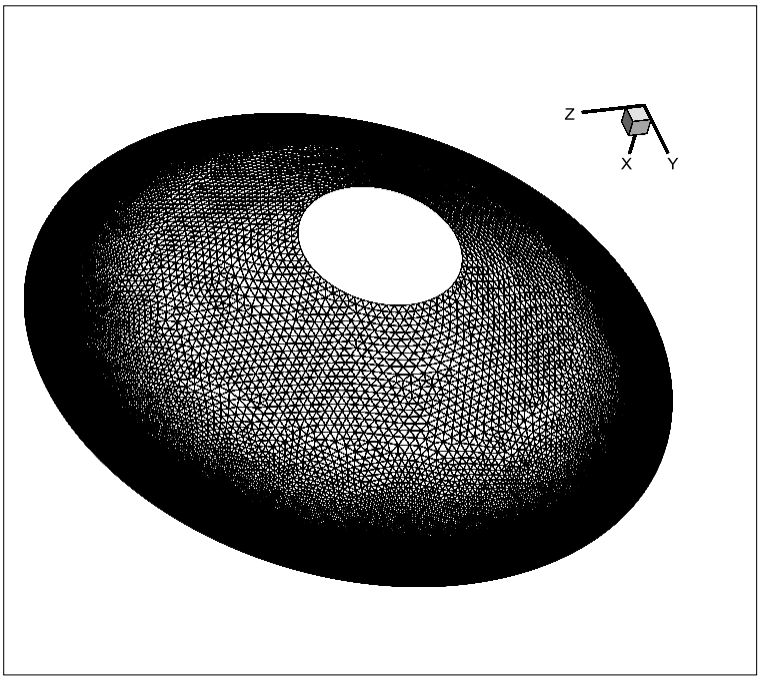

Figure 3: Deformable subsection of the HIAD surface mesh.

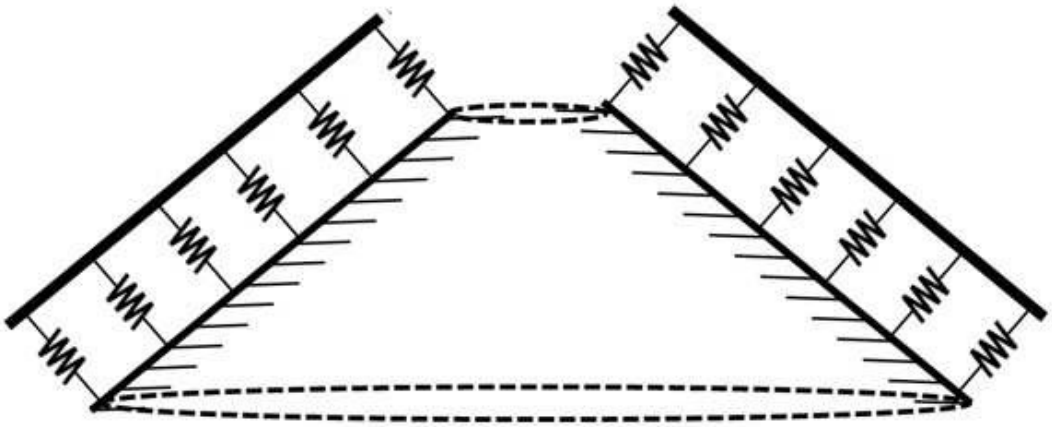

Figure 4: Elastically-supported conical shell model of the HIAD TPS.

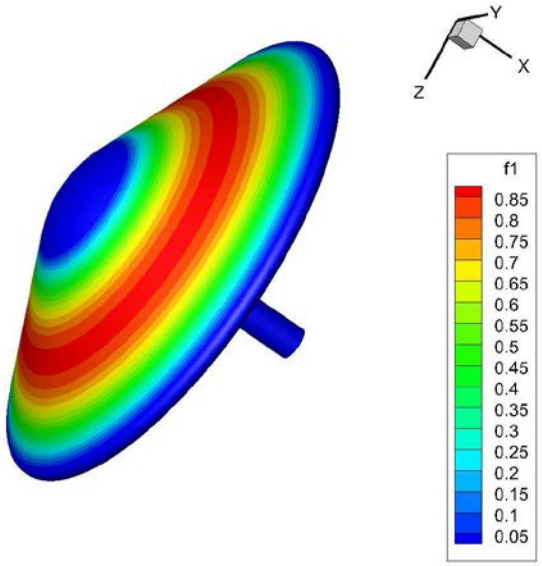

Figure 5: Assumed sinusoidal mode shape (n=1, k=0).

6.2 Results

Static and dynamic aeroelastic solutions were calculated at three points in a proposed HIAD re-entry trajectory. Initial re-entry at the edge of the atmosphere is characterized by hypersonic Mach numbers and almost no dynamic pressure, so it is highly unlikely that aeroelastic issues would be of concern in this portion of the trajectory. The final phase of re-entry near the Earth's surface is characterized by low subsonic Mach numbers and low dynamic pressures. If flutter were to occur here (also unlikely), it would not be of concern since most atmospheric deceleration has already occurred earlier in the trajectory. A peak in the dynamic pressure is seen at Mach 11, so this point will be examined for aeroelastic stability. In addition, trajectory points at Mach 1 and 2 will be considered since low supersonic and transonic flow regimes are often susceptible to limit cycle behavior. The trajectory point flow parameters are given in Table 2.

Table 2: Flow parameters for selected trajectory points.

Trajectory point	M_∞	q_∞ (PA)	V_∞ (m/s)	T_∞ (K)
1	1	350	317	242
2	2	575	640	256
3	11	1875 (peak q)	3470	238

6.2.1 Static Aeroelastic Solutions

Static aeroelastic solutions were computed using both linear and nonlinear structural solvers. The surface pressure coefficients, dimensional static pressures, and maximum deflections, sampled between

the last two elastic supports, are given in Table 3. Surface static pressure is greatest for trajectory point 3, at the peak free-stream dynamic pressure condition. The static deflection is greatest at this point as well. The maximum deflections calculated using the linear structural solver are similar to those calculated using the nonlinear solver at Mach 1 and 2, indicating that these conditions are within the (structurally) linear regime. At the Mach 11 peak dynamic pressure condition, the maximum nonlinear deflection is approximately 60 percent less than the linear result, indicating that the nonlinear structural effects are significant in this case. Comparisons of linear and nonlinear axial static deflection shapes are given in Figs. 6, 7, and 8. The slight differences in the deformation patterns can be attributed to the pressure-imposed membrane forces, which are only included in the nonlinear solutions.

Table 3: Static aeroelastic surface pressures and deflections, sampled between the last two (5^{th} and 6^{th}) elastic supports.

Trajectory Point	M_∞	$C_{Pmax,\ 5–6}$	$P_{s,max,\ 5–6}$ (Pa)	$w_{max,\ 5–6}$ (Linear) (m)	$w_{max,\ 5–6}$ (Nonlinear) (m)
1	1	0.6	660	8.66E–4	1.00E–3
2	2	1.125	827	2.51E–3	2.41E–3
3	11	1.45	2737	1.19E–2	6.31E–3

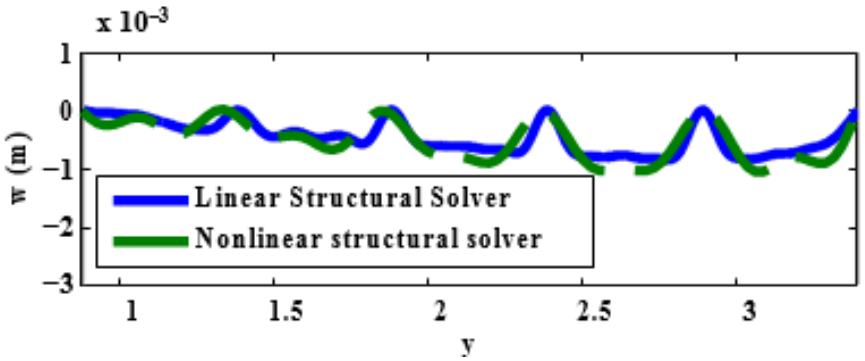

Figure 6: Comparison of the axial deflection shape calculated using the linear and nonlinear structural solvers, Mach 1 solution.

For the linear solver, steady state convergence of the static aeroelastic solutions is not time accurate, so a large time step can be selected, leading to convergence in relatively few iterations. The nonlinear solver is always time accurate, in that the time step must be commensurate with the *rtol* and *atol* tolerance parameters for the DLSODE solver. If these parameters are large enough, then the time step size can be increased, however, very large time steps generally result in numerical integration errors. A comparison of the linear and nonlinear static aeroelastic generalized displacements for the shell is given in Figs. 9 and 10. While these two cases have the same modal damping ratios the smaller time step in the nonlinear case allows the initial transients to be resolved. Additionally, though the characteristic dimensionless times for convergence for these cases are significantly different, the run time is nearly the same.

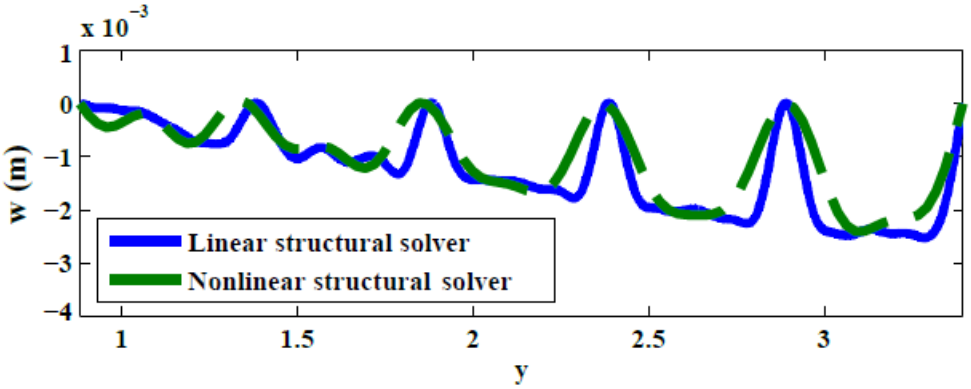

Figure 7: Comparison of the axial deflection shape calculated using the linear and nonlinear structural solvers, Mach 2 solution.

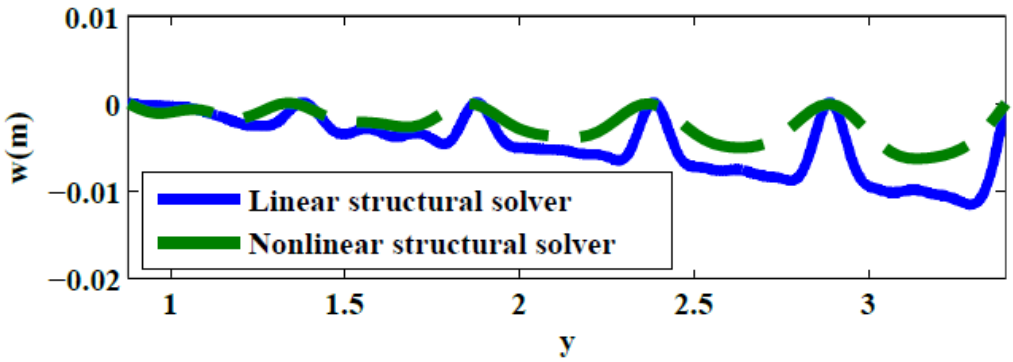

Figure 8: Comparison of the axial deflection shape calculated using the linear and nonlinear structural solvers, Mach 11 solution.

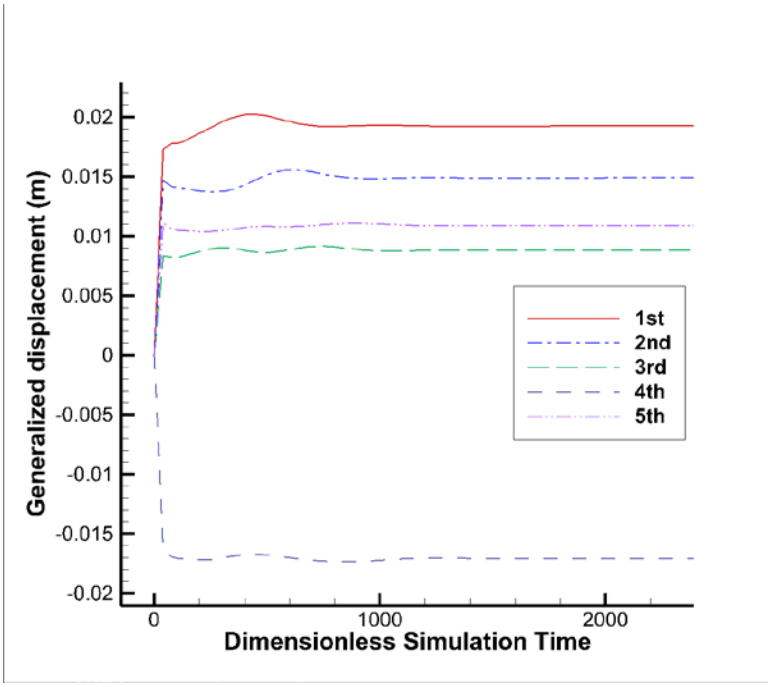

Figure 9: Static aeroelastic generalized displacements for the first 5 natural modes using the linear structural solver, Mach 2 solution.

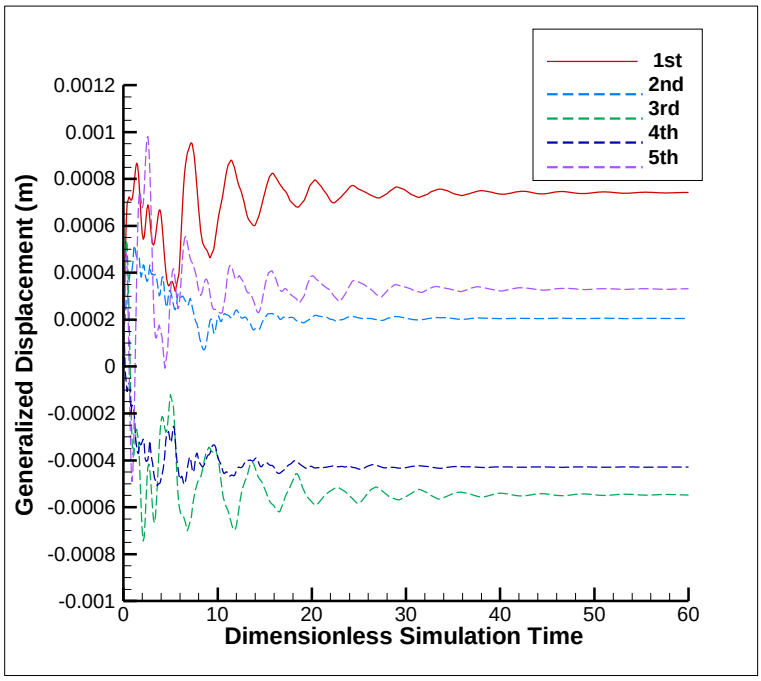

Figure 10: Static aeroelastic generalized displacements for the first 5 assumed sinusoidal modes using the nonlinear structural solver, Mach 2 solution.

6.2.2 Dynamic Aeroelastic Solutions

Linear dynamic aeroelastic solutions were computed at each of the three trajectory points in Table 2, and no flutter was observed, though sustained low amplitude oscillations are present at Mach 1, on the order of the shell thickness. The source of these oscillations are unlikely to be aeroelastic instability, but rather, excitations from noise in the flow. The time histories at each of the trajectory points are given in Fig. 11. Perturbation of the static aeroelastic solution results in (initially) large deflections with respect to the shell thickness, though these deflections are still orders of magnitude smaller than the shell radius. These time histories generally required at least three restarts and about two weeks to compute when using 156 CPU cores. It has been demonstrated previously that dynamic solutions can appear to decay initially and then grow to flutter or LCO, so enough time history must be computed to conclude that no flutter is present.

The free-stream dynamic pressure at each trajectory point was then increased incrementally, though not in intervals small enough to calculate accurately a flutter dynamic pressure. Values of approximately 10 times the trajectory dynamic pressures were used, and solutions remained stable. Based on these data, it is unlikely that a flutter condition can be achieved with the linear structural model and purely symmetric modes, though further investigation is needed.

Nonlinear dynamic aeroelastic solutions were also calculated at each of the three trajectory points, and the time histories are given in Fig. 12. Perturbation of the nonlinear static aeroelastic solutions results in smaller initial amplitudes than the linear solutions in Fig. 11, and response from higher structural modes is evident. This is because the structural equations are now coupled via the nonlinear terms that have been included. While the solutions at Mach 2 and 11 appear to decay, the Mach 1 solution exhibits some possible unstable behavior. While this is consistent with the fact that $q_\infty/\sqrt{(M_\infty^2 - 1)}$ increases rapidly at low supersonic and transonic Mach numbers, the instabilities seen here may not necessarily be physical. Non-physical explanations for this behavior include noise in the flow due to the turbulence model or flux limiter and possible insufficient spatial convergence. However, the nonlinear structural effects may also play a role. Recall that the nonlinear formulation includes the circumferential buckling (buckling/wrinkling) modes and membrane forces due to the mean flow static pressure, while the linear case that only includes the symmetric natural modes neglects the membrane forces. These components, in conjunction with the nonlinear structural terms, may be a factor in the unstable behavior in the transonic regime. We must also consider the nonlinear shock-structure interaction that could give rise to oscillatory motion.

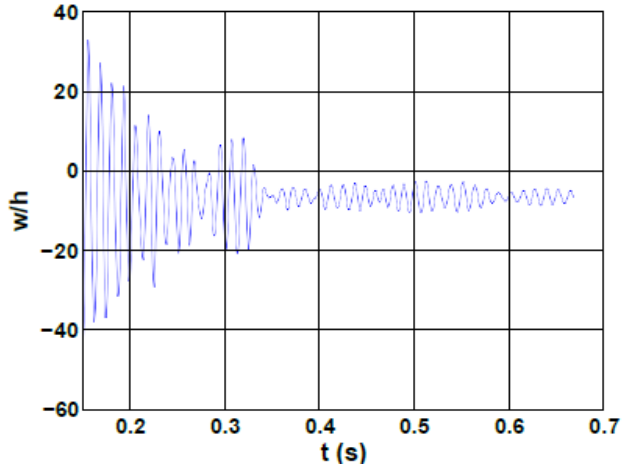

(a)Mach 1.

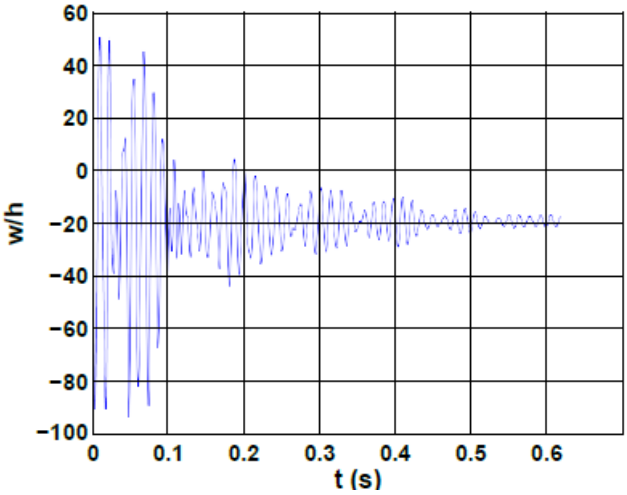

(b) Mach 2.

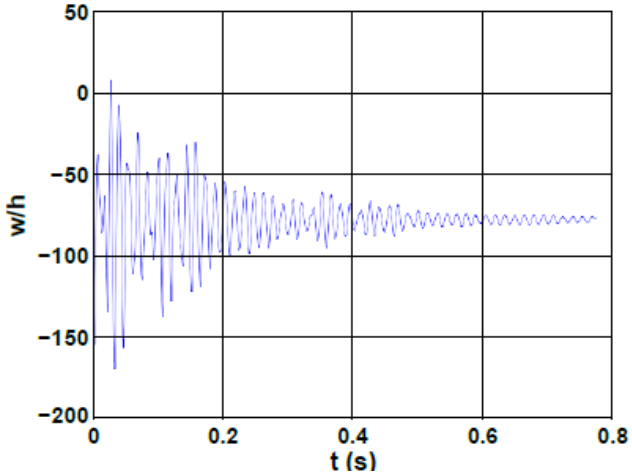

(c) Mach 11.

Figure 11: Deflection time histories at the three selected trajectory points using the linear structuralsolver.

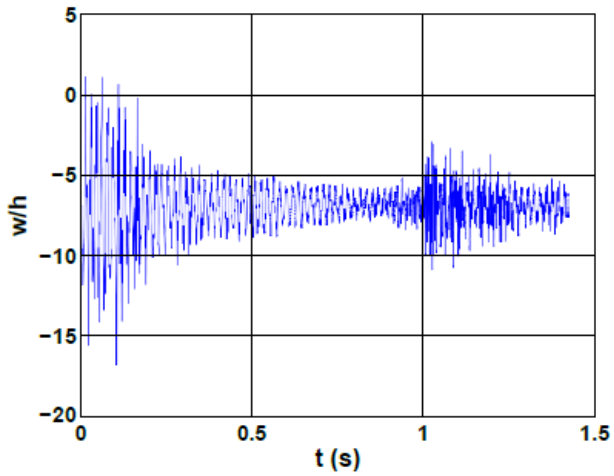

(a) Mach 1.

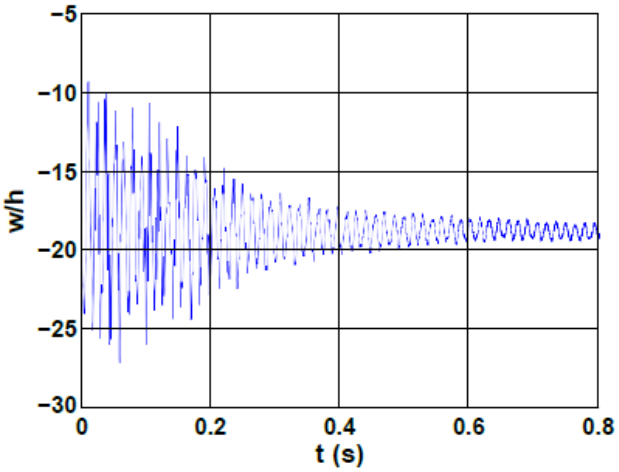

(b) Mach 2.

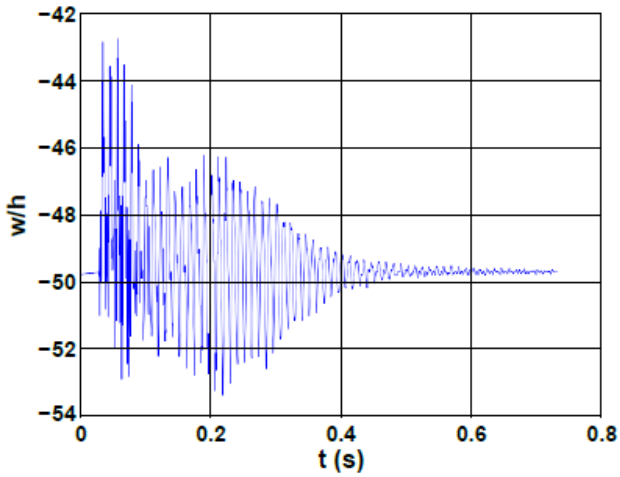

(c) Mach 11.

Figure 12: Deflection time histories at the three selected trajectory points using the nonlinear structural solver.

7 Concluding Remarks

A nonlinear modal structural solver has been integrated into FUN3D, allowing for aeroelastic analysis of structures with geometric nonlinearities. Three types of modal equations have been implemented, including those governing structures with in-plane displacements. A new input file is required to provide the structural solver parameters and nonlinear matrix and tensor coefficients. The ODEPACK DLSODE and the LAPACK DGESV functions are used to time-integrate the structural equations and invert linear systems where necessary. To incorporate these routines into FUN3D, a number of modifications to the compilation procedure are required and a step-by-step procedure has been provided.

A test case has also been included, demonstrating the functionality and capability of the nonlinear solver. We considered an elastically-supported conical shell model of the thermal protection system on the NASA Hypersonic Inflatable Aerodynamic Decelerator. Linear structural theory was used initially to determine the natural modes and frequencies for the unloaded shell, which were provided to the FUN3D linear structural solver. Nonlinear structural theory, the Rayleigh-Ritz method, and assumed sinusoidal modes were then used to derive a differential-algebraic system that could be solved using the new nonlinear solver. An analysis of the static aeroelastic solutions indicated that nonlinear structural effects were only significant at relatively high dynamic pressures where static deformations were large compared with the shell thickness. Both linear and nonlinear dynamic aeroelastic solutions generally decayed, though some possible instable behavior was observed in the transonic regime.

Finally, we also emphasize that the modifications to FUN3D discussed in this memorandum allow for expanded capabilities beyond that of just geometrically nonlinear structures. While a specific set of equations have been implemented in the source code, this new architecture actually allows for any modal structural equations of the form in Eq. 23. For example, external mechanical excitation, frictional forces, or other non-conservative forces could be added easily. In addition, other ODE solving capabilities are built into ODEPACK, including BDF methods for stiff problems and solvers for implicit systems.

References

1. R. T. Biedron, J. M. Derlaga, P. A. Gnoffo, D. P. Hammond, W. T. Jones, B. Kleb, E. M. Lee- Rausch, E. J. Nielsen, and M. A. Park, "FUN3D Manual: 12.5," *NASA TM*, no. 2014218520, 2014.

2. M. Schoenenberger, A. Dyakonov, P. Buning, W. Scallion, and J. V. Norman, "Aerodynamic challenges for the Mars Science Laboratory entry, descent and landing," 2009.

3. A. A. Dyakonov, M. Schoenenberger, W. I. Scallion, J. W. Van Norman, L. A. Novak, and C. Y. Tang, "Aerodynamic interference due to MSL reaction control system," *AIAA Paper*, vol. 3915, pp. 22–25, 2009.

4. R. E. Bartels, P. Chwalowski, S. J. Massey, J. Heeg, C. D. Wieseman, and R. E. Mineck, "Computational aeroelastic analysis of the ares launch vehicle during ascent," in *AIAA Applied Aerodynamics Conference, Chicago, June*, 2010.

5. V. N. Vatsa, M. R. Khorrami, M. A. Park, and D. P. Lockhard, "Aeroacoustic simulation ofnose landing gear on adaptive unstructured grids with fun3d," 2013.

6. N. L. R. Center, "FUN3D: Fully Unstructured Navier-Stokes." "http://fun3d.larc.nasa.gov/chapter-1.html#background/, December 2014. Online; accessed 19-December-2014.

7. J. W. Edwards, R. M. Bennett, W. Whitlow, and D. A. Seidel, "Time-marching transonic fluttersolutions including angle-of-attack effects," *Journal of Aircraft*, vol. 20, no. 11, pp. 899–906, 1983.

8. R. W. Brockett, *Finite Dimensional Linear Systems. Decision and Control*. John Wiley and Sons, 1970.

9. R. E. Bartels, C. L. Rumsey, and R. T. Biedron, "Cfl3d version 6.4-general usage and aeroelastic analysis," *NASA TM*, no. 2006-214301, 2006.

10. E. H. Dowell, *Aeroelasticity of plates and shells*. No. 1, Springer, 1974.

11. B. D. Goldman, R. C. Scott, and E. H. Dowell, "Nonlinear aeroelastic analysis of the HIAD TPS coupon in the NASA 8' High Temperature Tunnel: Theory and experiment," 2013 (submitted).

12. B. D. Goldman, E. H. Dowell, and R. C. Scott, "In-flight aeroelastic stability of the thermalprotection system on the NASA HIAD, Part II: Nonlinear theory and extended aerodynam-ics," in *56th AIAA/ASMe/ASCE/AHS/SC Structures, Structural Dynamics, and Materials Conference*, 2015.

13. A. C. Hindmarsh, "Serial Fortran solvers for ODE initial value problems," *URL: http://www. llnl. gov/CASC/odepack*, 2002.

14. E. Anderson, Z. Bai, C. Bischof, S. Blackford, J. Demmel, J. Dongarra, J. Du Croz, A. Green- baum, S. Hammerling, A. McKenney, *et al.*, *LAPACK Users' guide*, vol. 9. Siam, 1999.

15. R. H. MacNeal, *NASTRAN Theoretical Manual*, vol. 1. Scientific and Technical Informa- tion Office, National Aeronautics and Space Administration, 1972.

16. S. A. Rizzi and A. Przekop, "System identification-guided basis selection for reduced-order nonlinear response analysis," *Journal of Sound and Vibration*, vol. 315, no. 3, pp. 467–485, 2008.

17. A. A. Muravyov and S. A. Rizzi, "Determination of nonlinear stiffness with application to random vibration of geometrically nonlinear structures," *Computers & Structures*, vol. 81, no. 15, pp. 1513–1523, 2003.

18. S. A. Rizzi and A. A. Muravyov, "Equivalent linearization analysis of geometrically nonlinear random vibrations using commercial finite element codes," *NASA TP*, no. 2002-211761, 2002.

19. A. Radu, B. Yang, K. Kim, and M. Mignolet, "Prediction of the dynamic response and fatiguelife of panels subjected to thermo-acoustic loading," in *Proceedings of the 45th Structures, Structural Dynamics, and Materials Conference*, pp. 19–22, 2004.

20. G. Phlipot, X. Wang, M. P. Mignolet, L. Demasi, and R. Cavallaro, "Nonintrusive reduced order modeling for the nonlinear geometric response of some joined wings," in *Proceedings of the AIAA Science and Technology Forum and Exposition (SciTech2014), National Harbor, MD*, 2014.

21. A. C. Hindmarsh, "ODEPACK Source." "http://www.netlib.org/odepack/, April 2015. On- line; accessed 22-April-2015.

22. E. Anderson, "Lapack 3.5.0: Linear Algebra Package." "http://www.netlib.org/lapack/ explore-html/d8/d72/dgesv_8f.html, November 2013. Online; accessed 22-April-2015.

23. NASA, "HIAD image gallery." http://www.nasa.gov/offices/oct/stp/game_changing_development/HIAD/images.html.

REPORT DOCUMENTATION PAGE

Form Approved
OMB No. 0704-0188

1. REPORT DATE *(DD-MM-YYYY)*	2. REPORT TYPE	3. DATES COVERED *(From - To)*
01-02-2016	Technical Memorandum	

4. TITLE AND SUBTITLE

A Nonlinear Modal Aeroelastic Solver for FUN3D

5a. CONTRACT NUMBER

5b. GRANT NUMBER

5c. PROGRAM ELEMENT NUMBER

6. AUTHOR(S)

Goldman, Benjamin D.; Bartels, Robert E.; Biedron, Robert T.; Scott, Robert C.

5d. PROJECT NUMBER

5e. TASK NUMBER

5f. WORK UNIT NUMBER

432938.11.01.07.43.40.08

7. PERFORMING ORGANIZATION NAME(S) AND ADDRESS(ES)

NASA Langley Research Center
Hampton, VA 23681-2199

8. PERFORMING ORGANIZATION REPORT NUMBER

L-20621

9. SPONSORING/MONITORING AGENCY NAME(S) AND ADDRESS(ES)

National Aeronautics and Space Administration
Washington, DC 20546-0001

10. SPONSOR/MONITOR'S ACRONYM(S)

NASA

11. SPONSOR/MONITOR'S REPORT NUMBER(S)

NASA-TM-2016-219013

12. DISTRIBUTION/AVAILABILITY STATEMENT

Unclassified - Unlimited
Subject Category 02
Availability: NASA STI Program (757) 864-9658

13. SUPPLEMENTARY NOTES

14. ABSTRACT

A nonlinear structural solver has been implemented internally within the NASA FUN3D computational fluid dynamics code, allowing for some new aeroelastic capabilities. Using a modal representation of the structure, a set of differential or differential algebraic equations are derived for general thin structures with geometric nonlinearities. ODEPACK and LAPACK routines are linked with FUN3D,and the nonlinear equations are solved at each CFD time step. The existing predictor-corrector method is retained, whereby the structural solution is updated after mesh deformation. The nonlinear solver is validated using a test case for a flexible aeroshell at transonic, supersonic, and hypersonic flow conditions. Agreement with linear theory is seen for the static aeroelastic solutions at relatively low dynamic pressures,but structural nonlinearities limit deformation amplitudes at high dynamic pressures. No flutter was found at any of the tested trajectory points, though LCO may be possible in the transonic regime.

15. SUBJECT TERMS

Aeroelastic; Computational fluid dynamics; Deformation; Nonlinearity

16. SECURITY CLASSIFICATION OF:			17. LIMITATION OF ABSTRACT	18. NUMBER OF PAGES	19a. NAME OF RESPONSIBLE PERSON
a. REPORT	b. ABSTRACT	c. THIS PAGE			STI Help Desk (email: help@sti.nasa.gov)
					19b. TELEPHONE NUMBER *(Include area code)*
U	U	U	UU	35	(757) 864-9658